Journal of Catalysis 272 (2010) 275–286

Contents lists available at ScienceDirect

Journal of Catalysis

journal homepage: www.elsevier.com/locate/jcat

Effect of indium in trimetallic $Pt/Al_2O_3SnIn–Cl$ naphtha-reforming catalysts

Ali Jahel [a,b], Priscilla Avenier [a], Sylvie Lacombe [a,*], Josette Olivier-Fourcade [b], Jean-Claude Jumas [b]

[a] IFP-Lyon, Direction Catalyse et Séparation, Rond-point de l'échangeur de Solaize B.P. 3, 69360 Solaize, France
[b] ICG/AIME (UMR 5253 CNRS), Université Montpellier II CC 15-02, Place E. Bataillon, 34095 Montpellier Cedex 5, France

ARTICLE INFO

Article history:
Received 1 December 2009
Revised 12 March 2010
Accepted 10 April 2010
Available online 11 May 2010

Keywords:
Naphtha-reforming catalysts
Pt–Sn–In
Mössbauer spectroscopy
n-Heptane dehydrocyclization
Pt–Sn alloy
Electronic effect
Geometric effect

ABSTRACT

Trimetallic $Pt/Al_2O_3SnIn–Cl$ naphtha-reforming catalysts were characterized by ^{119}Sn Mössbauer spectroscopy, TPR, CO chemisorption, FTIR of adsorbed CO and NH_3-TPD. TPR traces indicate that indium facilitates tin reduction and strongly interacts with platinum as well. ^{119}Sn Mössbauer spectroscopy results show that addition of even small amount of In (0.06 wt.%) leads to the formation of a Pt_3Sn alloy. At higher indium loadings, higher amounts of Pt_xSn alloys of almost equal Pt and Sn atomic concentrations were detected. Indium also decreases the overall CO chemisorption capacity and provokes a modification of Pt electronic properties at the highest In loadings. A decrease in the acidity of the support in trimetallic catalysts is also observed by NH_3-TPD upon indium addition. These results correlate well with those from *n*-heptane-reforming reaction, showing that indium decreases catalyst's overall conversion and selectivity to C_1 and $C_3–C_4$ paraffins and increases isomerization selectivity.

1. Introduction

Catalytic naphtha reforming is a major petroleum refining process for the production of high octane hydrocarbons for automobile gasoline and aromatic hydrocarbons used in the petrochemical industry. Catalysts utilized in the process comprise two functions: the metallic function which consists of supported platinum particles on a porous support (usually chlorinated γ-alumina) and the acidic function which is the support itself. The major reactions that occur are the isomerization, dehydrogenation, and dehydrocyclization. However, undesired hydrogenolysis and hydrocracking reactions also occur and lead to gaseous $C_1–C_4$ hydrocarbons. The formation of methane is representative of hydrogenolysis reactions on platinum, which may also contribute to the coke deposition on the Pt surface and to subsequent loss in catalyst activity. The formation of $C_3–C_4$ hydrocarbons is representative of hydrocracking reactions on strong acidic sites. Both side reactions produce a decrease in liquid yield and stand in contrast to the very principle of catalytic reforming which is to reshape the structure of hydrocarbon chains increasing their octane values without changing their carbon number [1].

The first naphtha-reforming catalyst, Pt/Al_2O_3, was introduced in 1949 [2]. The process would later witness a big progress with the introduction of supported bimetallic-reforming catalysts, in which Pt is "promoted" by another metal, such as Re [3], Sn [4], Ge [5] and Ir [6]. Bimetallic catalysts have the advantage of better stabilities and enhanced selectivities to liquid reformate under reforming conditions. The exact role of these promoters which leads to such improvements is still a subject of controversy. Two effects are generally associated with the presence of a second metal. In the bimetallic $Pt–Sn/Al_2O_3Cl$, Sn atoms would exert a geometric effect by physically separating Pt atoms, thus reducing coalescence of the metallic phase during reaction/regeneration steps and reducing parasite hydrogenolysis reactions which demand the presence of large Pt ensembles [7,8]. Moreover, tin could cause a ligand effect [9], thus modifying the electronic properties of Pt active centres. This latter effect has been also described as a direct result of the formation of Pt_xSn alloys during reduction step, in which incorporated Sn atoms act as electron donors increasing the platinum electron density [10,11]. Others describe this electronic modification as resulting from the interaction of Pt with Sn ionic oxides produced during reduction and stabilized by the support [12,13]. Pt interaction with Sn ions mainly leads to electron-deficient Pt centres [14]. The controversy in reports describing the actual tin oxidation state and the nature of its interaction with the metal is due to differences in preparation methods, thermal treatments, supports and metal precursors used. Indeed, the state of tin after reduction and its interaction with platinum are governed by the strength of its interactions with the support. If the support is able to establish a strong interaction with tin, such as ceria, alumina, and titania, then it could hinder its total

* Corresponding author. Fax: +33 478 02 20 66.
E-mail addresses: ali.jahel@ifp.fr (A. Jahel), priscilla.avenier@ifp.fr (P. Avenier), sylvie.lacombe@ifp.fr (S. Lacombe), jolivier@univ-montp2.fr (J. Olivier-Fourcade), jumas@univ-montp2.fr (J.-C. Jumas).

0021-9517/$ - see front matter © 2010 Elsevier Inc. All rights reserved.
doi:10.1016/j.jcat.2010.04.007

reduction, whereas relatively inert supports like silica or carbon decreases the possibility of strong tin–support interactions [15]. The effect of tin addition on the acidity of the alumina support is well documented, whereby tin addition generally decreases the number of strong acidity sites, which catalyses undesired hydrocracking reactions and favours by consequence the presence of medium and mild acidity sites, which catalyse desired skeletal rearrangements [16–18].

Despite the beneficial promotional aspects of tin, coke formation is not completely eliminated, and catalysts still exhibit short life times and must undergo continuous or frequent regenerations to maintain their activity [19]. Recently, trimetallic naphtha-reforming catalysts comprising the Pt–Sn system modified by the addition of a second promoter have received close attention. A number of studies have been already carried out on multimetallic reforming catalysts, such as Pt–Sn–Ir/Al_2O_3–Cl [20] and Pt–Sn–Re/Al_2O_3–Cl [18,21,22]. These catalysts represent a new generation of naphtha-reforming catalysts. In this vein also, the preparation of trimetallic Pt–Sn–In/Al_2O_3–Cl catalysts has been the subject of several patents [23,24], which claim an improvement on C5+ liquid products yield compared to the Pt–Sn system. However, few scientific reports exist on the effect of indium to the Pt–Sn/Al_2O_3–Cl catalyst. Lately, Bocanegra et al. [25] carried out a study on Pt–Sn–In/$MgAl_2O_3$ catalysts and found that indium addition remarkably enhances the catalyst stability and inhibits undesired hydrogenolysis reactions. Many studies were also carried out on the role of indium in bimetallic Pt–In/Al_2O_3–Cl catalysts [26–29]. This work aims at studying the effect of indium on the acidic and metallic functions in trimetallic Pt–Sn–In catalysts on chlorinated γ-Al_2O_3 carrier. For this purpose, we have prepared and characterized trimetallic Pt/Al_2O_3SnIn–Cl catalysts with variable indium loadings. Tin and indium have been introduced to the alumina support via co-precipitation (sol–gel method), thus providing a material with a high chemical homogeneity [30]. Reference monometallic as well as bimetallic supports and catalysts were also prepared and characterized. The samples were characterized by TPR to examine In reducibility as well as its effect on the reducibility of other metals. The effect of indium addition on the consequent Pt–Sn interactions was investigated using ^{119}Sn Mössbauer spectroscopy. Characterization of Pt–Sn-reforming catalysts by this technique has been already reported and proved to be advantageous concerning the information provided on chemical structure, oxidation state and local symmetry of observed Sn species [31]. The effect of indium on the electronic and geometric properties of platinum was studied using FTIR of adsorbed CO and CO chemisorption. Indium effect on the catalyst's acidic properties was investigated by NH_3-TPD. Finally, the influence of indium on the catalytic performance was investigated using *n*-heptane reforming as a probe reaction.

2. Experimental

2.1. Catalyst preparation

Supports were initially prepared by co-precipitating known amounts of $In(NO_3)_3.5H_2O$ and/or $SnCl_2.2H_2O$ with $Al(NO_3)_3$ at 30 °C with controlled stirring using NH_4NO_3 and NH_4OH as precipitation agents. The concentration of the alumina precursor was equivalent to 60 g/l Al_2O_3 with a molar ratio NH_4NO_3/Al_2O_3 = 0.2. A sufficient amount of NH_4OH was added during about 30 min in order to obtain a pH around 8. The obtained precipitate was filtered, washed with distilled water and then put in the form of pellets. These were then dried at 80 °C in an oven during 12 h and then heated at a rate of 3 °C/min–740 °C whereby they were subjected to calcination in dry air during 4 h.

Catalysts were prepared by introducing proper amounts of Pt and Cl precursors (H_2PtCl_6, $5H_2O$, and HCl) by the incipient wetness technique on the γ-alumina support already doped with In and/or Sn to obtain about 0.3 and 1.5 wt.% of Pt and Cl respectively. The support was placed in a water volume corresponding to a ratio $V_{water}/m_{support}$ = 4.5 ml/g (water volume to support mass ratio). Pt impregnation was carried out overnight on an agitation table. The obtained catalyst was filtered, washed with distilled water and dried in oven at 120 °C during 12 h. The catalyst was finally calcined in a tubular reactor (2 h, 520 °C) in dry air flow (rate = 1 - l h^{-1} g^{-1}). The chlorine content was adjusted to 1 wt.% by treatment in wet air (0.8 wt.% H_2O) at 520 °C. All final catalysts contained comparable amounts of Pt, Sn, and Cl (about 0.3 wt.%. Sn and Pt, and about 1 wt.%. Cl, as determined by X-ray fluorescence spectroscopy). The indium loading in the trimetallic catalysts was varied between 0.06 and 0.59 wt.% (Table 1). Preparation of reduced catalyst samples was carried out by heating pre-calcined samples in a tubular reactor during 2 h at 500 °C under pure hydrogen flow (rate = 1 l g^{-1} h^{-1}). For simplicity, Pt non-containing supports are referred to as Al_2O_3Sn–Cl, Al_2O_3In–Cl and Al_2O_3SnIn–Cl. Trimetallic catalysts are denoted in the text by Pt/Al_2O_3SnIn(*x*)–Cl with *x* = In loading in wt.%. Bimetallic catalysts are simply referred to as Pt/Al_2O_3Sn–Cl or Pt/Al_2O_3In–Cl.

2.2. Textural properties of the support

Surface area (S_{BET}) for previously dried samples during two hours at 350 °C was determined by nitrogen isothermal adsorption on an Asap 2420 multi-post apparatus (Micromeritics). Porous volume of dried supports/catalysts was measured by mercury porosimetry on an Autopore IV apparatus (Micromeritics).

2.3. Temperature programmed reduction (TPR)

TPR experiments were carried out on an Autochem(II) apparatus (Micromeritics) using about 0.8 g of catalyst. Temperature was first increased to 150 °C (8 °C/min) under argon stream (10 ml/min) whereby catalyst was dried during 1 h. After cooling to room temperature and switching to hydrogen (5% H_2 in argon, 10 ml/min), temperature was increased up to 1000 °C (8 °C/min). Hydrogen consumption (in a.u.) during the temperature profile was determined by a TCD device connected to the apparatus.

2.4. ^{119}Sn Mössbauer spectroscopy

^{119}Sn Mössbauer spectra were recorded at room temperature in the transmission mode on a standard EG&G spectrometer in the constant acceleration mode, by using a $Ca^{119m}SnO_3$ source of 10 mCi nominal activity. The velocity scale was calibrated by means of a room temperature spectrum of α-Fe recorded with a ^{57}Co(Rh) source. The hyperfine parameters δ (isomer shift) and Δ

Table 1
Metal and chlorine loadings (obtained by X-ray fluorescence) of the different prepared samples.

Support/catalyst	Pt (wt.%)	Sn (wt.%)	In (wt.%)	Cl (wt.%)
Al_2O_3Sn–Cl	–	0.32	–	1.02
Al_2O_3In–Cl	–	–	0.39	1.00
Al_2O_3SnIn–Cl	–	0.30	0.39	1.02
Pt/Al_2O_3–Cl	0.30	–	–	0.98
Pt/Al_2O_3Sn–Cl	0.30	0.32	–	1.02
Pt/Al_2O_3In–Cl	0.29	–	0.39	1.06
Pt/Al_2O_3SnIn(0.06)–Cl	0.30	0.29	0.06	1.00
Pt/Al_2O_3SnIn(0.21)–Cl	0.28	0.33	0.21	1.01
Pt/Al_2O_3SnIn(0.39)–Cl	0.30	0.30	0.39	1.00
Pt/Al_2O_3SnIn(0.59)–Cl	0.30	0.30	0.59	1.03

(quadrupole splitting) were determined by fitting the Lorentzian lines to the experimental data by using the ISO programme [32]. All isomer shifts are given with respect to the room temperature spectrum of $BaSnO_3$. The characterized quantity of each sample was typically around 2 g. The effective thickness of all absorbers was in the range of 0.5–1.0 mg $^{119}Sn\ cm^{-2}$. All catalysts were characterized in two forms: calcined and reduced. Calcined samples were obtained after calcination at 520 °C for 2 h in air stream ($1\ l\ h^{-1}\ g^{-1}$). Reduced sample were obtained by reduction at 500 °C for 2 h in hydrogen stream ($1\ l\ h^{-1}\ g^{-1}$). The reduction was performed in special U-shaped reduction cells adapted for Mössbauer spectroscopy measurements. Once reduction was completed, the cell was neutralized and sealed under vacuum.

2.5. FTIR of chemisorbed CO

Samples were analysed by IR on a Nexus 1 spectrometer. Self-supported wafers of about 30 mg were prepared and dried under vacuum at 150 °C and 500 °C (1 and 10 h respectively). Samples were then reduced at 500 °C by introducing excess hydrogen into the IR chamber (450 m bar, 30 min). Hydrogen was then evacuated by applying secondary vacuum to the cell for 30 min. The reduction steps were repeated four times. CO was then introduced to the sample at room temperature by successive pulses of increasing volumes until saturation and IR–CO spectra were recorded after each pulse. In order to determine the $\nu(CO–Pt^0)$, the method of M. Primet [33] was followed to avoid CO–CO dipole coupling that usually leads to observation of higher frequencies. IR spectra were recorded in the transmission mode with an accumulation time of 100 s and a resolution of $4\ cm^{-1}$ after CO thermo-desorption at 25, 50, 75, 100, and 150 °C respectively (15 min each). Obtained frequencies were then plotted as a function of temperature and the plot extrapolated to zero-CO-coverage at which the $\nu(CO–Pt^0)$ was determined.

2.6. CO chemisorption

Experiments were carried out on a chemisorption equipment designed ad hoc. The catalyst was placed in a quartz reactor, and temperature was increased to 150 °C (5 °C/min) in He ($1\ l\ h^{-1}\ g^{-1}$) whereby the catalyst was dried for 1 h. Then, temperature was increased to 500 °C (5 °C/min) whereby the gas was switched to hydrogen ($1\ l\ h^{-1}\ g^{-1}$) and the catalyst reduced for 2 h. Adsorbed hydrogen was then desorbed in He at the same temperature for 1 h. After cooling to room temperature, CO pulses ($0.24\ cm^3$) were introduced to the catalyst until surface saturation. Non-chemisorbed CO was quantitatively determined by a catharometer device placed at the reactor exit.

2.7. STEM analysis

Grinded reduced samples were suspended in ethanol and stirred continuously in an ultrasonic bath. The resulting suspension was deposited on a copper grid with a holey-carbon-film support, and the alcohol was evaporated. STEM experiments were performed on a TECNAI & JEM 2100F microscope working at 200 kV. This allowed estimating the particle size range on the different reduced catalysts.

2.8. Temperature programmed desorption (TPD) of NH_3

TPD experiments were carried out on an Autochem(II) apparatus (Micromeritics) connected to a TCD apparatus using about 0.5 g of calcined catalyst. Temperature was first increased to 500 °C (8 °C/min) at a rate of 8 °C/min in helium flow (50 ml/min). The gas was switched to hydrogen (50 ml/min), and the catalyst was reduced during 2 h. After cooling to 100 °C in helium flow (50 ml/min), the catalyst was activated at this temperature during 30 min by adsorption of NH_3 (10 vol.% in He) at a rate of 50 ml/min. Physisorbed NH_3 was then flushed at the same temperature in helium flow (50 ml/min) over 1 h. Temperature programmed desorption was then carried out by heating the sample from 100 °C to 500 °C at a rate of 8 °C/min in helium flow (10 ml/min). Parallel analysis by a quadrupole mass spectrometer (Pfeiffer) showed that NH_3 was the only desorbing species below 500 °C.

2.9. n-Heptane reforming

The test reaction was carried out in the continuous flow mode in a fixed bed tubular reactor at 470 °C and total pressure of 8 bar, with a hydrogen-to-hydrocarbon molar ratio H_2:HC equal to 3 and a WHSV of $2\ h^{-1}$. Prior to the test, catalysts (about 2 g each) were reduced *in situ* under hydrogen flow (500 °C, 2 h). The analysis of reactants and reaction products was carried out using an AGILENT 6890 gas chromatography apparatus connected on-line and equipped with a flame ionization detector and a capillary column of copper tube coated with squalene (J and W Scientific DB-1). Total conversion (X) and the yields to each reaction product (Y_i) were calculated on carbon basis. Conversion was defined as:

$$X = \frac{HC^i - HC^0}{HC^i}$$

where HC^i is the concentration of the fed hydrocarbon at the reactor inlet, and HC^0 is the concentration of the non-reacted hydrocarbon at the reactor outlet. Selectivity (S_i) to product i was calculated as follows:

$$S_i = \frac{Yield(i)}{X} = \frac{A_i f_i n_i}{X M_i \sum A_i f_i n_i / M_i}$$

where A_i is the area of the chromatographic peak of the product i; f_i is its response factor; n_i is the number of carbon atoms of i, and M_i is its molecular weight. Hydrogenolysis selectivity only includes the selectivity to methane formation. Selectivity to isomerization includes only selectivities to i-C_7 and i-C_6 hydrocarbons, while hydrocracking selectivity included selectivity to C_3 and C_4 hydrocarbons. Dehydrocyclization selectivity is represented by the selectivity to toluene formation.

3. Results and discussion

3.1. Textural properties of the support

All obtained supports possessed a specific surface area (S_{BET}) and porous volume of 190 (±10) m^2/g and 0.53 (±0.02) ml/g respectively, typical of mesoporous materials, irrespective of the tin and/or indium content. Additionally, experiments performed on catalysts after Pt impregnation and reduction in hydrogen at 500 °C confirmed that no significant changes in specific surface areas and porous volumes took place.

3.2. Temperature programmed reduction (TPR)

Fig. 1 shows the TPR traces of reference monometallic Al_2O_3In–Cl, Al_2O_3Sn–Cl and bimetallic Al_2O_3SnIn–Cl supports. The indium reduction profile consists of two regions: a lower reduction region peaking at 430 °C and a higher reduction region peaking at 850 °C, with a little shoulder near 740 °C. This reduction profile of alumina supported In oxides has been previously observed in studies carried out by Park et al. [34] and Perdigon-Melon et al. [35] and was considered to result from the reduction of In oxide particles of different sizes with more or less strong interaction with the

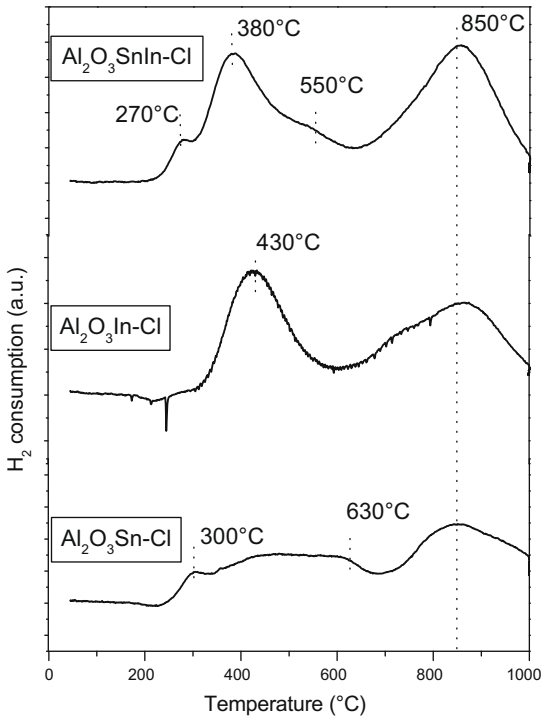

Fig. 1. TPR traces of monometallic Al_2O_3Sn–Cl and Al_2O_3In–Cl and bimetallic Al_2O_3SnIn–Cl supports.

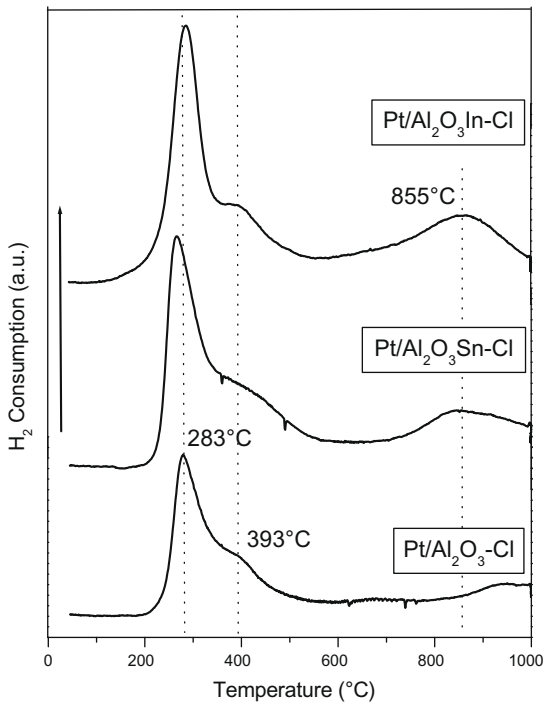

Fig. 2. TPR traces of monometallic Pt/Al_2O_3–Cl and bimetallic Pt/Al_2O_3In–Cl and Pt/Al_2O_3Sn–Cl catalysts.

support. Hence, the reduction of In oxides weakly bonded to the support proceeds in the first reduction region, and species strongly interacting with the support (probably In-aluminates) are reduced at the highest temperatures. The Al_2O_3Sn–Cl support shows a wide trace of weak hydrogen consumption starting near 240 °C and ending at about 700 °C, with a shoulder at 300 °C plus a second reduction zone peaking at 850 °C. The two regions correspond to the reduction of Sn species of different interaction strengths with the alumina support. The higher reduction region (at higher temperatures) is probably due to the reduction of refractory Sn-aluminates, which might have been formed during support calcination. This observation is expected since Sn oxides are generally accepted to be in close interaction with the alumina support after calcination [9]. Surprisingly, the TPR trace of the bimetallic Al_2O_3SnIn–Cl support shows that reduction of both metallic oxides in the lower temperature region occurs at lower temperatures. The shoulder seen for tin reduction in the Al_2O_3Sn–Cl support at 300 °C is now shifted to 270 °C, and the first indium reduction peak seen before at 430 °C for the Al_2O_3In–Cl support is now shifted to 380 °C. Moreover, an additional shoulder appears at 550 °C. This shoulder most likely corresponds to the reduction of Sn species of stronger interaction with the support, which in the absence of indium are reduced at higher temperatures (near 630 °C). Considering that the promoter–support interaction strength has a big influence on promoter's reduction [15,17], the fact that the reduction of both metallic oxides is shifted to lower temperatures in the bimetallic support suggests that a bigger fraction of both metals is in a relatively weak interaction with alumina due to competition for reactive alumina sites, resulting in easier reduction.

Fig. 2 shows the TPR traces of monometallic Pt/Al_2O_3–Cl and bimetallic Pt/Al_2O_3Sn–Cl and Pt/Al_2O_3In–Cl catalysts. The TPR trace of Pt/Al_2O_3–Cl consists of a consumption peak at 283 °C with a shoulder near 393 °C, which is similar to previously reported results [36]. The first well-defined peak corresponds to the reduction of $PtOCl_2$ species on the surface and the shoulder at 393 °C is most likely associated with the reduction of Pt species in stronger interaction with the support [37,38]. The Pt/Al_2O_3Sn–Cl catalyst shows a similar profile in the platinum reduction region, but a noticeable increase in the hydrogen consumption is observed compared to the Pt/Al_2O_3–Cl catalyst. It is noted that a tin fraction is simultaneously reduced with platinum, indicating close Pt–Sn proximity, possibly leading to the reduction of some Sn oxides into the metallic state. The signal peaking near 860 °C, already observed for the monometallic Al_2O_3Sn–Cl support, is also observed for this catalyst. This probably corresponds to the reduction of Sn species in the form of Sn–O–Sn and/or Sn–O–Al oxides. The bimetallic Pt/Al_2O_3In–Cl catalyst also shows a similar increase in hydrogen consumption in the Pt reduction region, particularly near 300 °C, and the peak near 860 °C also appears. This indicates that a fraction of In initially being reduced at 430 °C in the monometallic sample (Fig. 1) is now reduced near 280 °C and, to a lesser extent, near 390 °C. Such a shift in the reduction temperature of In is typical of close Pt–In intimacy, possibly in the form of Pt_xIn alloys.

Fig. 3 shows the TPR traces of Pt/Al_2O_3Sn–Cl and trimetallic $Pt/Al_2O_3SnIn(x)$–Cl catalysts. It is observed that in the case of trimetallic catalysts hydrogen consumption in the region of platinum reduction increases as the indium content increases. The increase is seen in both reduction zones near 270 and 380 °C. While the increase in hydrogen consumption in the first zone occurs at the same temperature, the reduction peak seen near 420 °C for the bimetallic Pt/Al_2O_3Sn–Cl catalyst is further shifted to lower temperatures in the presence of In. The shift becomes clearer for catalysts with the highest In contents (0.39 and 0.59 wt.%), for which the shoulder appears near 360 °C. This indicates that the added indium not only interacts with platinum but also provokes a synergetic effect on Sn, facilitating its reduction in the trimetallic system similarly as in the bimetallic Al_2O_3SnIn–Cl support. This could also mean that the presence of indium possibly reinforces Pt–Sn interactions. The position of the higher temperature region seems unaffected by the presence of indium (850 °C), but the hydrogen consumption increases as In loading increases. This is expected and similar to TPR results obtained for reference supports and bimetallic catalysts.

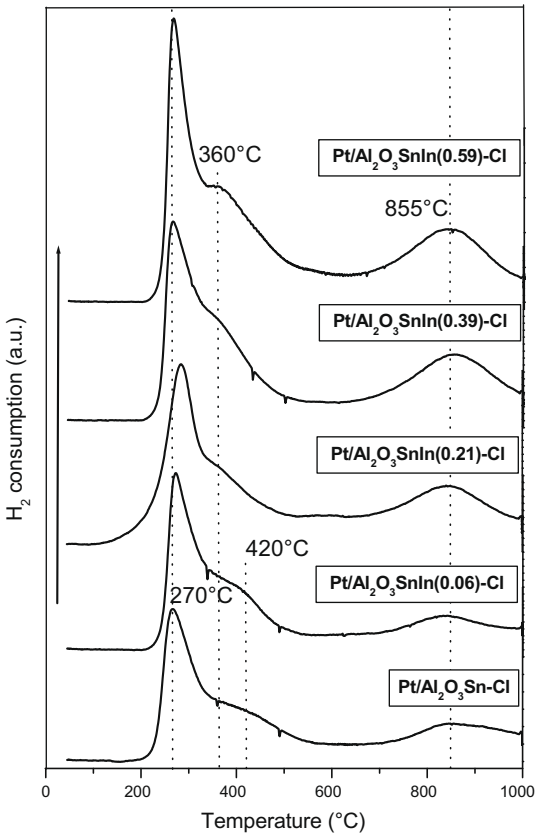

Fig. 3. TPR traces of bimetallic $Pt/Al_2O_3Sn–Cl$ and trimetallic $Pt/Al_2O_3SnIn–Cl$ catalysts.

3.3. ^{119}Sn Mössbauer spectroscopy

Table 2 summarizes the hyperfine parameters δ (isomer shift in mm s^{-1}) and Δ (quadrupole splitting in mm s^{-1}) of Sn species observed by ^{119}Sn Mössbauer spectroscopy for calcined samples. All catalysts as well as the reference support $Al_2O_3SnIn–Cl$ possess Mössbauer spectra comprising two sub-spectra of two different types of Sn^{IV} oxides. Ratios with which Sn phases are formed are calculated starting from the contributions of phases to spectra, since the constant **f** (Lamb–Mössbauer factor), necessary for phase quantification, is not calculated in this work. Classification of oxidized/reduced Sn species in bimetallic $Pt–Sn/Al_2O_3–Cl$ has been reported in previous studies [31,39]. Generally, three types of Sn^{IV} oxides on the surface as well as in the bulk of γ-Al_2O_3 can be distinguished by Mössbauer spectroscopy. The first with $0.40 < \Delta < 0.80$ normally called SnO_2 1 is an SnO_2 like lattice with Sn–O–Sn bridges. The second species labelled Sn^{IV} 2 with a higher quadrupole splitting ($0.80 < \Delta < 1.50$) consists of a bimetallic lattice of tin with another metal such as Al or Pt. This lattice is most probably at the interface of the SnO_2 1 lattice with the support and/or the platinum, thus explaining the more important asymmetric charge distribution in the Sn–O bond in Sn–O–M (M = Pt, Al) reflected by a higher quadrupole splitting. Only these two types were found to be present in our calcined samples. A third type of Sn oxides, called SnO_2 0, was observed in other studies on the surface of $Sn/Al_2O_3–Cl$ supports prepared by impregnation/deposition of tin on the surface [31,39]. This oxide corresponds to small rather isolated, molecule-like particles that are not embedded in the alumina matrix, but instead comprising small octahedral SnO_6 clusters on the outermost sphere of a bigger particle. The absence of this oxide in all samples is thus directly resulting from the co-precipitation method where tin oxides are strongly interacting with the support with a fraction of the oxide present at the surface, most likely as particles partially embedded in the alumina matrix. Although In addition causes weaker Sn-alumina interactions as concluded from TPR results, spectra obtained for the two supports $Al_2O_3Sn–Cl$ and $Al_2O_3SnIn–Cl$ in the oxidized state do not reveal an obvious difference concerning the environment of Sn species. Sn^{IV} 2 and SnO_2 1 are formed in approximately 1:4 ratio irrespective of indium presence (Table 2). On the other hand, this ratio is close to 2:3 for all Pt-containing samples, except for $Pt/Al_2O_3SnIn(0.21)–Cl$ which has a ratio close to 1:3 (Table 2). Comparison of ^{119}Sn Mössbauer spectra of Pt-containing catalysts and corresponding Pt-non-containing supports (i.e. before Pt impregnation) reveals some differences (Fig. 4). Pt Impregnation on the $Al_2O_3SnIn–Cl$ support to yield the $Pt/Al_2O_3SnIn(0.39)–Cl$ catalyst leads to the modification of the Sn^{IV} 2 (Sn–O–M) to SnO_2 1 (Sn–O–Sn) ratio from 1:4 to 2:3 approximately. Evidently, a fraction of tin oxides (Sn–O–Sn) is present on the surface, and a fraction of platinum oxides is deposited in the proximity of these particles thus transforming some of these oxides into the Sn–O–Pt phase upon Pt impregnation and further calcination. This is informative on the fact that in the case of the bimetallic $Pt/Al_2O_3Sn–Cl$ catalyst, the reduction of a fraction of Sn species is shifted to lower temperatures, compared to the $Al_2O_3Sn–Cl$ support, as observed through TPR experiments (Fig. 1). This fraction of Sn species is thus the fraction in close contact with platinum. Therefore, tin is present in the alumina bulk (due to the preparation method of the support) as well as on the alumina surface.

Fig. 5 schematically represents the characterized SnO_2 1 and Sn^{IV} 2 oxides. The former species are likely to form small partially

Table 2
^{119}Sn Hyperfine parameters δ = isomer shift (mm s^{-1}) and Δ = quadrupole splitting (mm s^{-1}) of observed Sn species and their contribution to spectra of calcined samples recorded at room temperature.

Sample	δ	Δ	FWHM[a]	C[b] (%)	Attribution	Absorption (%)
$Al_2O_3Sn–Cl$	0.002(2)	0.69(4)	0.93(9)	76	SnO_2 1	2.24
	0.10(6)	1.30(1)	0.93(9)	24	Sn^{IV} 2	
$Al_2O_3SnIn–Cl$	−0.02(1)	0.59(2)	0.92(3)	78	SnO_2 1	2.39
	0.10(5)	1.28(8)	0.92(2)	22	Sn^{IV} 2	
$Pt/Al_2O_3Sn–Cl$	−0.03(1)	0.50(2)	0.83(2)	64	SnO_2 1	3.48
	0.06(2)	1.20(3)	0.83(7)	36	Sn^{IV} 2	
$Pt/Al_2O_3SnIn(0.06)–Cl$	−0.03(2)	0.48(3)	0.87(2)	63	SnO_2 1	2.81
	0.03(3)	1.10(6)	0.87(2)	37	Sn^{IV} 2	
$Pt/Al_2O_3SnIn(0.21)–Cl$	−0.02(1)	0.53(2)	0.83(2)	72	SnO_2 1	3.33
	0.02(3)	1.20(6)	0.83(0)	28	Sn^{IV} 2	
$Pt/Al_2O_3SnIn(0.39)–Cl$	−0.02(2)	0.41(4)	0.87(3)	62	SnO_2 1	2.27
	0.002(0)	1.17(7)	0.87(3)	38	Sn^{IV} 2	
$Pt/Al_2O_3SnIn(0.59)–Cl$	−0.02(2)	0.47(2)	0.84(2)	61	SnO_2 1	3.0
	0.02(2)	1.09(4)	0.84(8)	39	Sn^{IV} 2	

[a] Full width at half maximum.
[b] Contribution to total spectrum.

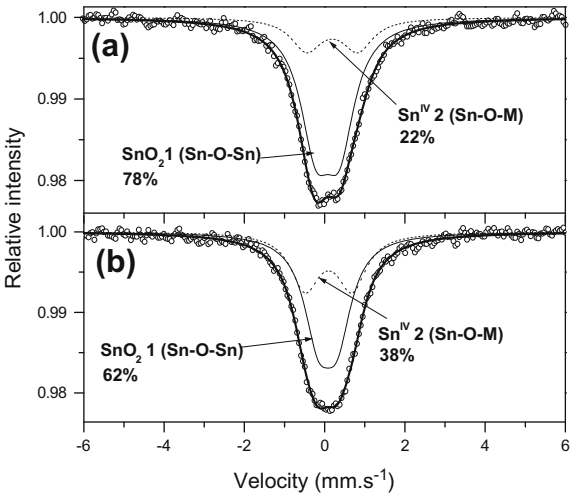

Fig. 4. ^{119}Sn Mössbauer spectra of: (a) the $Al_2O_3SnIn(0.39)$–Cl support and (b) the $Pt/Al_2O_3SnIn(0.39)$–Cl catalyst.

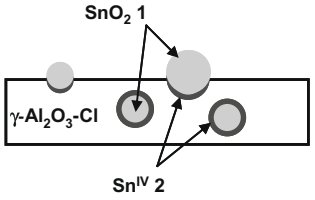

Fig. 5. Surface and bulk Sn oxides present on an Al_2O_3Sn–Cl support prepared by co-precipitation.

embedded particles in the alumina surface. Sn^{IV} 2 species would constitute the interfacial layer with the alumina bulk. These species also constitute similar interfacial layers around other particles fully embedded in the alumina matrix, since tin was introduced to the support by the sol–gel technique. The increase of In loading does not further modify the composition of Sn oxides in the oxidized state. All Trimetallic catalysts appear to have similar ratios of Sn^{IV} oxides irrespective of the In loading (Table 2).

Reduction at 500 °C under hydrogen affects both Sn^{IV} 2 and SnO_2 1 phases. For the Al_2O_3SnIn–Cl bimetallic support, both oxides showed lesser contributions to the ^{119}Sn spectrum (Fig. 6). Sn^{IV} 2 and SnO_2 1 species are formed in a ratio of 1:3 after reduction. Two types of Sn^{II} oxides are also identified. The so-called Sn^{II} 2a (δ = 3.12 mm s^{-1}, Δ = 2.5 mm s^{-1}) and Sn^{II} 2b (δ = 3.62 mm s^{-1}, Δ = 0.90 mm s^{-1}) are formed in a 2:3 ratio. The former oxide comprises a Sn^{II}–O–M (M = Pt, In, Al) structure [31]. The absence of platinum in this sample implies that the other metal can be either In or Al. The presence of another metal at the end of the oxygen bridge and the perturbation of the local symmetry around the tin atom explain the relatively high quadrupole splitting value calculated for this oxide. The lower isomer shift relative to that of the Sn^{II} 2b oxide indicates a stronger covalent character of the Sn–O bond in the Sn–O–M bridge, which in turn indicates a smaller s electronic density at the tin nucleus. The latter oxide called Sn^{II} 2b corresponds to a Sn^{II} oxide with only Sn–O–Sn bridges, which justifies its smaller quadrupole splitting [31]. Therefore, in the absence of platinum, tin reduction does not proceed below the oxidation state (II). This is consistent with the observations of Burch et al. [9] and is mainly due to a strong Sn-alumina interaction appearing after calcination. The presence of indium does not push further the tin reduction to the metal state but however leads to a more efficient reduction to the second oxidation state of tin, with a

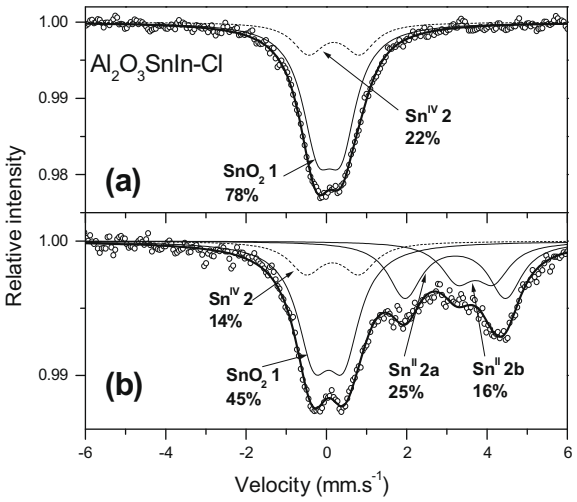

Fig. 6. ^{119}Sn Mössbauer spectra of Al_2O_3SnIn–Cl bimetallic support: (a) calcined at 520 °C in dry air flow and (b) reduced at 500 °C in H_2 stream.

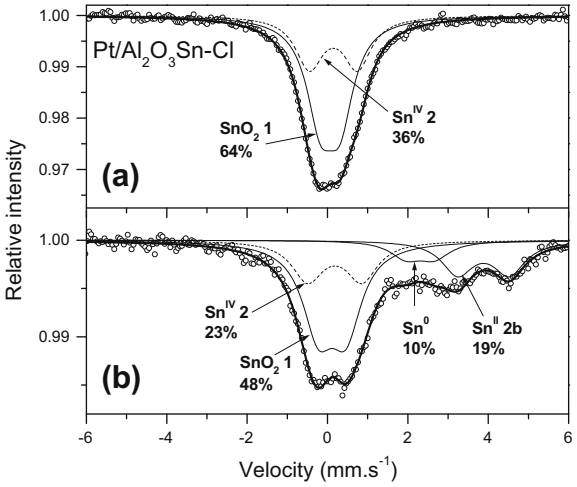

Fig. 7. ^{119}Sn Mössbauer spectra of Pt/Al_2O_3Sn–Cl bimetallic catalyst: (a) calcined at 520 °C in dry air flow and (b) reduced at 500 °C in H_2 stream.

Sn^{IV}–Sn^{II} ratio of 3:2 compared to a ratio of 3:1 [31] in the absence of In. The most affected Sn^{IV} species upon reduction appears to be the SnO_2 1 oxide. This is consistent with the fact that tin atoms in such an oxide particle are in weak contact with the support, unlike in the case of Sn^{IV} 2 oxides where Al atoms are practically occupying sites of the first coordination shell of Sn atoms.

Reduction of the bimetallic Pt/Al_2O_3Sn–Cl catalyst at 500 °C also leads to the formation of two new Sn species from the initially two coexisting Sn^{IV} phases (Fig. 7). The Sn^{IV} 2 and the SnO_2 1 phases initially present in a 1:2 ratio contribute less to the Mössbauer spectrum after reduction, but their ratio is however little changed. The first new phase observed at δ = 3.8 mm s^{-1} and Δ = 1.29 mm s^{-1} (Table 3) lies in the natural range of hyperfine parameters of Sn^{II} 2b oxides. The second Sn phase observed at δ = 2.22 and Δ = 0.7 mm s^{-1} is almost at the lower limit of isomer shifts observed for Sn-rich Pt_xSn alloys, usually observed at δ values between 2.3 and 2.5 mm s^{-1} [31]. Unlike these alloys of null Δ values, this phase shows a small Δ value of 0.7 mm s^{-1}, indicating a δ^+ charge that could be originating from interactions of tin atoms with alumina and a certain perturbation in its local symmetry. Therefore, this phase is most probably an un-alloyed metallic tin phase, i.e. a bimetallic aggregate or a solid solution of tin in

Table 3
^{119}Sn Hyperfine parameters δ = isomer shift (mm s^{-1}) and Δ = quadrupole splitting (mm s^{-1}) of observed Sn species and their contribution to spectra of reduced samples (500 °C, 2 h, H_2 flow) recorded at room temperature.

Sample	δ	Δ	FWHM[a]	C[b] (%)	Attribution	Absorption (%)
Al_2O_3SnIn–Cl	−0.04(1)	0.74(1)	0.99(2)	45	SnO_2 1	1.33
	0.06(0)	1.32(3)	0.99(0)	14	Sn^{IV} 2	
	3.12(2)	2.50(3)	0.99(7)	25	Sn^{II} 2°	
	3.62(4)	0.90(4)	0.99(2)	16	Sn^{II} 2b	
Pt/Al_2O_3Sn–Cl	0.02(3)	0.70(5)	0.95(0)	48	SnO_2 1	1.7
	0.09(6)	1.35(1)	0.95(2)	23	Sn^{IV} 2	
	3.80(3)	1.29(4)	0.95(7)	19	Sn^{II} 2b	
	2.22(7)	0.70(5)	0.95(4)	10	Sn^0	
Pt/Al_2O_3SnIn(0.06)–Cl	0.03(2)	0.67(1)	1.02(0)	39	SnO_2 1	1.46
	0.09(3)	1.21(4)	1.02(0)	29	Sn^{IV} 2	
	3.66(4)	1.34(5)	1.02(0)	27	Sn^{II} 2b	
	1.67(0)	0	1.02(4)	5	Pt_3Sn	
Pt/Al_2O_3SnIn(0.21)–Cl	0.00(1)	0.67(0)	1.04(0)	42	SnO_2 1	1.32
	0.05(3)	1.18(3)	1.04(0)	25	Sn^{IV} 2	
	3.64(3)	1.19(3)	1.04(0)	25	Sn^{II} 2b	
	1.78(0)	0	1.04(2)	8	$Pt_{2.6}Sn$	
Pt/Al_2O_3SnIn(0.39)–Cl	0.02(0)	0.71(1)	0.86(0)	44	SnO_2 1	1.14
	0.09(2)	1.27(3)	0.86(0)	27	Sn^{IV} 2	
	3.69(3)	1.21(4)	0.86(2)	20	Sn^{II} 2b	
	1.93(0)	0	0.86(2)	9	PtSn	
Pt/Al_2O_3SnIn(0.59)–Cl	0.01(0)	0.70(1)	0.94(0)	44	SnO_2 1	1.17
	0.10(3)	1.12(4)	0.94(0)	22	Sn^{IV} 2	
	3.60(3)	1.19(4)	0.94(2)	23	Sn^{II} 2b	
	1.82(0)	0	0.94(3)	11	PtSn	

[a] Full width at half maximum.
[b] Contribution to total spectrum.

platinum. Solid solutions of tin in platinum have been widely pointed at [9,14], but their position in the phase transition into pure Pt-n alloys is not clearly known. Srinivasan et al. [40] reported that such a phase could result from the incomplete decomposition of a solid solution of the oxide phase upon reduction or calcination, but concluded that metallic tin is not attained after reduction if tin was introduced by the sol–gel technique. Indeed, our results show that even when tin is introduced to the alumina support via this technique, a metallic tin phase could be formed after reduction in hydrogen in the presence of platinum.

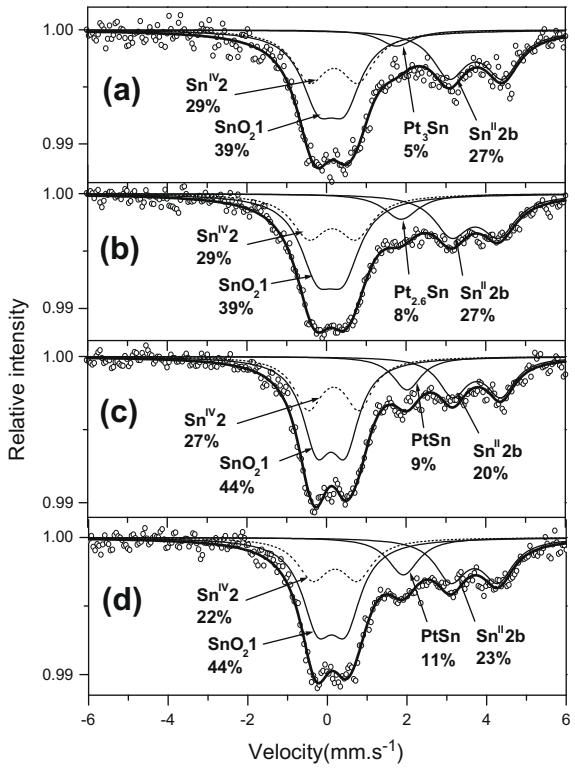

Fig. 8. ^{119}Sn Mössbauer spectra of reduced trimetallic catalysts (500 °C, H_2): (a) Pt/Al_2O_3SnIn(0.06)–Cl; (b) Pt/Al_2O_3SnIn(0.21)–Cl; (c) Pt/Al_2O_3SnIn(0.39)–Cl; and (d) Pt/Al_2O_3SnIn(0.59)–Cl. The intensity of the Pt_xSn alloy signal is seen to increase with In loading.

Reduction of the trimetallic Pt/Al_2O_3SnIn(0.06)–Cl catalyst also affords Sn^{IV}, Sn^{II}, and Sn^0 phases. Both Sn^{IV} phases are partially reduced with a more pronounced reduction impact on the SnO_2 1 phase. The only Sn^{II} phase present after reduction is the Sn^{II} 2b phase (Fig. 8a). All isomer shifts and quadrupole splitting values calculated for the appearing Sn^{IV} and Sn^{II} species are in normal expected ranges of hyperfine parameters. Surprisingly, a pure Pt_xSn alloy phase, not observed in the case of the reduced bimetallic Pt/Al_2O_3Sn–Cl catalyst, is identified at δ = 1.67 mm s^{-1} with a zero quadrupole splitting (Table 3). The position of the singlet as well as its zero Δ value corresponds to a pure Pt_3Sn alloy. Formation of Pt–Sn alloys after reduction has been previously reported in ^{119}Sn Mössbauer spectroscopy studies of bimetallic Pt–Sn catalysts prepared by co-impregnation [11], controlled surface reactions [39,41–43] and successive impregnations [10,44]. However, the formation of such alloys have been denied by Mössbauer spectroscopy when tin was added to the catalyst via the co-precipitation of Sn and Al oxides [31,40]. Unexpectedly, all trimetallic Pt–Sn–In catalysts reported in this study are shown to contain Pt_xSn alloys after the reduction step. Reduction mostly affects the SnO_2 1 oxide and the Sn^{II} 2b is the only Sn^{II} phase formed. The Sn^{IV} 2 phase, rather comprising Sn–O–Al oxides, is little affected by the reduction. The ratio Sn^{IV}: Sn^{II} is close to 3.5: 1 for all trimetallic catalysts. At 0.21 wt.% of In, the alloy phase singlet is slightly more intense and appears at isomer shift δ = 1.78 mm s^{-1} (Fig. 8b). According to the results of Olivier-Fourcade et al. [31] this phase contains a tin atomic concentration intermediate between those of Pt_3Sn and PtSn alloys. Increasing the In loading (catalysts with 0.39 and 0.59 wt.%) apparently increases the intensity of the formed

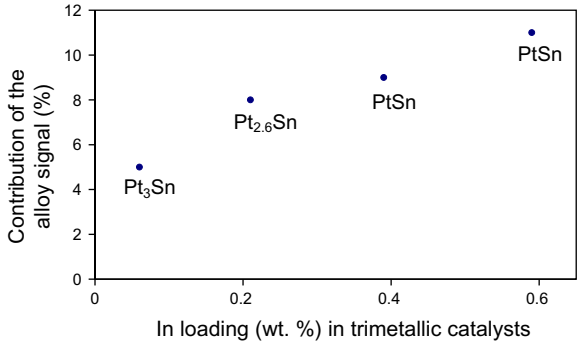

Fig. 9. Composition of Pt_xSn alloys and their signal contribution to the total ^{119}Sn Mössbauer spectra of trimetallic catalysts as a function of In loading.

alloy signal (Figs. 8 and 9). Furthermore, the positions (Table 3) of the corresponding alloy signals formed in these catalysts (1.93 and 1.82 mm s^{-1} respectively) indicate that they contain almost equal amounts of platinum and tin [31] (Table 3). These results are in good agreement with our conclusions obtained from TPR experiments, showing that addition of In shifts further the reduction of Sn oxides to lower temperatures (Fig. 3). The added In occupies coordinatively unsaturated sites on the surface of the alumina support, which are normally occupied by Sn oxides in the absence of In. As the In loading increases, more Sn oxides are in a weaker interaction with alumina, and Pt–Sn alloying becomes possible, with more tin atomic concentration in the formed alloys (Fig. 9). In the absence of indium, tin reduction to the metallic state is possible, but the interaction of Sn^0 atoms with alumina disfavours the formation of pure Pt_xSn alloys.

3.4. FTIR–CO

In order to investigate the possibility that In addition provokes a modification of platinum electronic properties, catalysts were characterized by FTIR spectroscopy of adsorbed CO. Table 4 includes the results of FTIR–CO experiments carried out on reduced samples at 500 °C after thermal desorption of pre-adsorbed CO at 150 °C. Thermal desorption provides a rather accurate measure of $\nu(CO–Pt^0)$ and has been used in previous studies [26,33]. It allows to avoid the modification of the $\nu(CO–Pt^0)$ singleton due to dipole–dipole interactions occurring between adsorbed CO molecules, which usually lead to higher frequencies [33]. CO linearly adsorbed on terrace sites on Pt crystal faces is normally seen as a peak at 2075 cm^{-1} [45,46]. Passos et al. [26] found that this peak is shifted to nearly 2063 cm^{-1} when the average size of Pt particles decreases assigning the new peak to CO linearly adsorbed on Pt particles that do not have extended crystal faces because of their small size and morphologies. When Pt particles have a relatively higher size, CO can form bridges on Pt atoms, which is seen as a small peak near 1835 cm^{-1} [26,45]. For all our samples including the monometallic platinum catalyst, this latter peak was not observed, suggesting good platinum dispersion. The singleton frequency observed for the monometallic Pt/Al_2O_3–Cl catalyst is equal to 2076 cm^{-1}. The bimetallic Pt/Al_2O_3Sn–Cl catalyst shows only one peak at 2075 cm^{-1} excluding that tin addition induces an electronic effect on Pt. The major promoting mechanism of tin in the bimetallic catalyst thus appears to be geometric. On the other hand, the Pt/Al_2O_3In–Cl catalyst shows a small shift (7 cm^{-1}) in the observed frequency (2069 cm^{-1}) relative to the Pt/Al_2O_3–Cl catalyst. This could be due to a smaller average size of Pt particles in the bimetallic Pt–In system. It could also be due to an electronic effect resulting from strong Pt–In interactions observed by TPR, possibly in the form of Pt_xIn alloys. We tend to consider this shift as a result of a small change in the Pt particle size in the presence of In, since the observed difference is not very important.

Trimetallic catalysts with relatively low In loadings (0.06 and 0.21 wt.%) do not show considerable decrease in the observed CO frequency compared to the bimetallic Pt/Al_2O_3In–Cl, even though the presence of In has led to the formation of Pt_xSn alloys. The platinum electronic properties in these catalysts are thus more or less comparable to the electronic properties of platinum in the bimetallic catalysts. At higher indium loadings (starting from 0.39 wt.%), the frequency of adsorbed CO considerably decreases to reach a minimal value of 2053 cm^{-1} for the catalyst with the highest indium loading. These catalysts were also shown to contain increasing amounts of Pt–Sn alloys of almost equal Pt and Sn atomic concentrations (Fig. 9). Verbeek and Sachtler [47] characterized Pt electronic properties in Pt–Sn alloys by temperature-programmed desorption of CO and found that while maximum desorption temperature of CO adsorbed on bulk Pt_3Sn alloys was only little different than that of pure Pt powder, a larger temperature shift was observed for the PtSn bulk alloy. Their main conclusion was that Sn exerts an electronic (ligand) effect on Pt when the amount of Sn in the Pt–Sn alloy increases. Our results agree with this conclusion, and therefore an electronic effect of tin on platinum in these catalysts could be assigned. The absence of a frequency shift in the case of the bimetallic Pt/Al_2O_3Sn–Cl catalyst could thus be explained by the fact that the observed metallic tin was rather unalloyed with platinum.

3.5. CO chemisorption

CO chemisorption results are listed in Table 4. The molar CO/Pt ratio could be directly related to the Pt dispersion, but in the case of multimetallic catalysts, it can be affected by several factors other than Pt accessibility, such as electronic effects of metallic promoters which can alter the CO chemisorption capacity of platinum [48]. Addition of Sn or In to Pt/Al_2O_3–Cl leads to a decrease in the CO/Pt ratio. This could be due to physical blockage induced by proximate Sn and In ad-atoms. The decrease however seems slightly more important in the case of In addition, in agreement with other studies suggesting a more homogenous blocking effect of indium on platinum compared to tin [26,27]. In trimetallic

Table 4
($CO–Pt^0$) frequencies (cm^{-1}) from FTIR–CO spectroscopy, CO chemisorption and NH_3-TPD results for different samples.

	Pt/Al_2O_3–Cl	Pt/Al_2O_3In–Cl	Pt/Al_2O_3Sn–Cl	Trimetallic $Pt/Al_2O_3SnIn(x)$–Cl catalysts			
				x^d = 0.06	x^d = 0.21	x^d = 0.39	x^d = 0.59
$\nu(CO–Pt^0)$[a]	2076	2069	2075	2068	2070	2065	2053
CO/Pt[b]	0.79	0.70	0.76	0.51	0.46	0.42	0.35
NH_3 (μmol/g)[c]	–	–	4.70	4.60	4.30	4.10	4.27

[a] Obtained after thermal desorption of CO on reduced samples (cm^{-1}).
[b] Molar ratio.
[c] Total amount of desorbed NH_3 between 100 and 500 °C from NH_3-TPD.
[d] In content (wt.%) in trimetallic catalysts.

catalysts, indium appears to decrease the catalysts adsorption capacity even at very low contents (0.06 wt.%). The CO/Pt ratio then progressively decreases with increasing In loadings to reach a minimum at the highest loading (0.59 wt.%). This could be due to physical blockage by Sn^0 atoms in Pt_xSn alloys or by Sn ions (as deduced from Mössbauer spectroscopy results), and In atoms possibly forming alloys with Pt. Furthermore, an electronic effect is also observed in the case of the $Pt/Al_2O_3SnIn(0.39)$–Cl and $Pt/Al_2O_3SnIn(0.59)$–Cl catalysts, as deduced from IR–CO spectroscopic results. Therefore, it is proposed that the decrease in their CO chemisorption capacities results from a combined geometric/electronic effect of indium and tin atoms. For the $Pt/Al_2O_3SnIn(0.06)$–Cl and $Pt/Al_2O_3SnIn(0.21)$–Cl catalysts which contain Pt_xSn alloys, the important decrease in their chemisorption capacities relative to the Pt/Al_2O_3Sn–Cl, in the absence of modification of Pt electronic properties, might indicate that Sn atoms in Pt_xSn alloys could induce more geometric effects than the non-alloyed Sn^0 phase formed on the Pt/Al_2O_3Sn–Cl catalyst.

3.6. STEM analysis

Fig. 10 shows selected STEM images of reduced monometallic Pt/Al_2O_3–Cl, bimetallic Pt/Al_2O_3Sn–Cl and trimetallic Pt/Al_2O_3Sn In(0.39)–Cl and $Pt/Al_2O_3SnIn(0.59)$–Cl catalysts. The monometallic and bimetallic catalysts show a narrow particle size distribution between 0.6 and 1.1 nm. No particle size changes are observed after Sn addition. On trimetallic catalysts, the particle size distribution is slightly shifted to higher size values (between 0.5 and 1.5 nm at 0.39 wt.% In and between 0.6 and 1.4 nm at 0.59 wt.% In respectively). This could be related to the formation of bimetallic aggregates (Pt–Sn or Pt–In) of a relatively higher size after addition of In. These results are in agreement with our CO chemisorption results, indicating that the added In decreases the chemisorption capacity of Pt.

3.7. Temperature-programmed desorption (TPD) of NH_3

The effect of indium addition on the acidic properties of the catalyst was investigated using TPD of NH_3. Fig. 11 shows the NH_3 desorption traces obtained for the Pt/Al_2O_3Sn–Cl and trimetallic $Pt/Al_2O_3SnIn(x)$–Cl catalysts. Table 4 also lists the total amount of desorbed NH_3 (μmol/g) for the different catalysts. All trimetallic catalysts are seen to possess NH_3-TPD traces less intense than that of the bimetallic Pt/Al_2O_3Sn–Cl catalyst, and the intensity of the trace is obviously decreased by further amounts of In with the exception of the $Pt/Al_2O_3SnIn(0.59)$–Cl catalyst, whose NH_3-TPD trace appears to be slightly more intense than that of Pt/Al_2O_3 SnIn(0.39)–Cl. This could be due to partial In crystallization at relatively higher loadings, which leads to less poisoning of sites on the support, as suggested by Benitez et al. [49] who found similar observations on indium effects by TPD of pyridine. The total number of acidic sites is thus decreased by the presence of In (Table 4) in agreement with the results of Passos et al. [28] and Rodríguez-González et al. [50]. It is worth mentioning that the decrease in the quantity of the desorbed NH_3 is seen at lower (<350 °C) and higher temperature (>350 °C) regions, indicating that the population of strong acidity sites has been decreased by indium presence as well. Indium aluminates might have been formed upon thermal

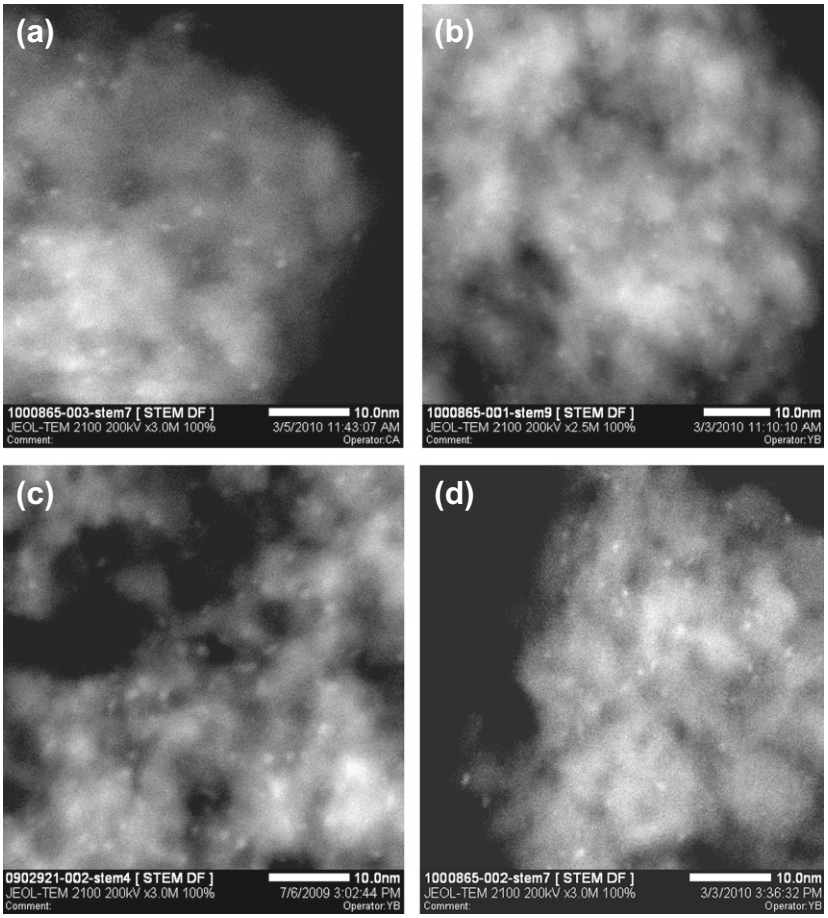

Fig. 10. Selected STEM images of reduced catalysts: (a) Pt/Al_2O_3–Cl; (b) Pt/Al_2O_3Sn–Cl; (c) $Pt/Al_2O_3SnIn(0.39)$–Cl; and (d) $Pt/Al_2O_3SnIn(0.59)$–Cl.

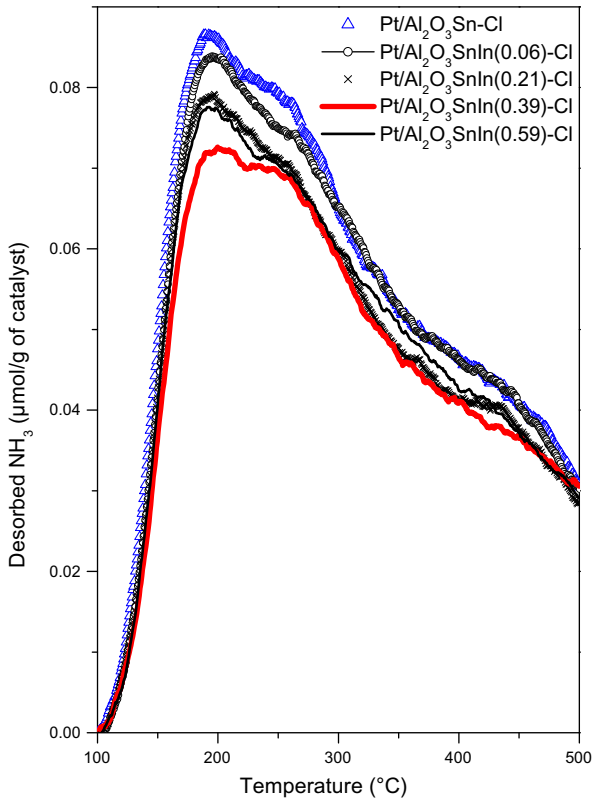

Fig. 11. NH_3-TPD traces of bimetallic $Pt/Al_2O_3Sn–Cl$ and trimetallic $Pt/Al_2O_3SnIn–Cl$ catalysts.

treatments during catalyst preparation leading to the neutralization of some acidic sites of the alumina support. This suggestion would be supported by the TPR traces of trimetallic catalysts (Fig. 3), which show an increase in the intensity of the higher temperature reduction zone (850 °C) with increasing In contents.

3.8. n-Heptane reforming

Table 5 shows the *n*-heptane conversion for the bi- and trimetallic catalysts at 470 °C after 22 h on stream. Compared to the bimetallic $Pt/Al_2O_3Sn–Cl$ catalyst, the $Pt/Al_2O_3In–Cl$ catalyst presents a lower conversion. This is in agreement with our CO chemisorption results, suggesting a stronger blocking effect on platinum in the case of indium, and in agreement with other studies [26,27]. Unlike tin which usually strongly interacts with alumina after the calcination step, indium oxides are generally easily reduced to the metal state in the presence of platinum [35]. Our TPR trace obtained for the bimetallic $Pt/Al_2O_3In–Cl$ suggests that indium is strongly interacting with the metal function of the catalyst (Fig. 2).

Table 5
Catalytic performance for bi- and trimetallic catalysts in the *n*-heptane-reforming reaction (at 470 °C, 8 bar, molar ratio $H_2:C_7H_{16} = 3$ and WHSV = 2 h^{-1}) after 22 h on stream.

Catalyst	Conversion (%)	Selectivity (%)			
		C_1	$C_3–C_4$	*i*-C_6–*i*-C_7	Toluene
$Pt/Al_2O_3In–Cl$	88.6	1	10.5	42	21.5
$Pt/Al_2O_3Sn–Cl$	93.3	1	14.7	31.2	21.8
$Pt/Al_2O_3SnIn(0.06)–Cl$	93.0	1	13.5	32.2	21.5
$Pt/Al_2O_3SnIn(0.21)–Cl$	90.4	0.8	11.3	41.7	19.9
$Pt/Al_2O_3SnIn(0.39)–Cl$	89.5	0.8	10	44.1	21.1
$Pt/Al_2O_3SnIn(0.59)–Cl$	84.8	0.6	7	56.8	16.9

For trimetallic catalysts, addition of low indium amounts (0.06 wt.%) slightly decreases the catalyst conversion, and increasing the In content leads to a further decrease in the catalyst activity. The greatest activity loss observed at the biggest indium content (0.59 wt.%) is consistent with our CO chemisorption results, showing a decrease in chemisorption capacity at increasing indium contents and our STEM results (Fig. 10) showing a slight increase in the particle size distribution at highest In loadings. Decrease in conversion is also related to the loss of acid alumina sites due to In presence as suggested by our NH_3-TPD results (Fig. 11). Benitez et al. [49] found that indium addition to trimetallic $Pt–Re–Sn/Al_2O_3–Cl$ and $Pt–Re–Ge/Al_2O_3–Cl$ catalysts decreases the total conversion in cyclohexane dehydrogenation and *n*-heptane-reforming reactions. They attributed this to the loss of acid sites by the mild basic In oxides and to a blocking effect, whereby In atoms decrease the accessibility of Pt atoms and therefore decrease the dehydrogenation activity (structure non-sensitive reaction). Our results are in agreement with such conclusions.

Table 5 also summarizes the catalysts selectivities to different reaction products after 22 h on stream. The selectivity to C_1 was chosen to represent hydrogenolysis activity. Both bimetallic $Pt/Al_2O_3Sn–Cl$ and $Pt/Al_2O_3In–Cl$ show comparable hydrogenolysis selectivities. On the other hand, methane selectivity tends to decrease when indium is added to $Pt/Al_2O_3Sn–Cl$ even at low indium content (0.06 wt.%). The lowest methane selectivity is observed at the highest In content (0.59 wt.%). This can be explained by an "ensemble effect" [51] provoked by indium through the formation of Pt–Sn alloys and possibly Pt–In alloys, as deduced from our ^{119}Sn Mössbauer spectroscopy and TPR results respectively. In these intermetallic species, tin or indium atoms separate neighbouring Pt atoms without totally blocking their accessibility, thus preventing multi-adsorption of carbon chains. Since hydrogenolysis requires the adsorption of two adjacent carbon atoms over neighbouring Pt sites (structure sensitive), the latter effect leads to a decrease in hydrogenolytic activity [49]. Similar results were reported by demonstrating a decrease of hydrogenolytic activity when adding indium to trimetallic $Pt–Re–Sn/Al_2O_3–Cl$ and $Pt–Re–Ge/Al_2O_3–Cl$ catalysts even at small amounts (0.1 wt.%) [49]. Our results are also in good agreement with the conclusions of Bocanegra et al. [25] on the passivation of hydrogenolysis sites induced by indium addition to $PtSn/MgAl_2O_4$ catalysts even at low loadings (0.13 wt.%) as well as with the results of Passos et al. [26,27] and Mériaudeau et al. [52,53] stating for the passivation by In of hydrogenolysis sites in bimetallic Pt–In catalysts. Furthermore, an electronic effect could be added in the case of trimetallic catalysts with high In loadings (0.39 and 0.59 wt.%), as our FTIR–CO results suggested (Table 4).

Results in Table 5 clearly show that as the indium content in trimetallic catalysts increases, lower selectivities to hydrocracking products (C_3 and C_4 hydrocarbons) and higher selectivities to isomerization products are obtained with increasing In loadings compared to the bimetallic $Pt/Al_2O_3Sn–Cl$ catalyst. Both isomerization and hydrocracking reactions are controlled by the acid function of the catalyst: isomerization reactions are favoured on mild acidity sites, whereas hydrocracking reactions become more favoured on strong acidity sites [16]. Our results obtained from NH_3-TPD show that indium addition to $Pt/Al_2O_3Sn–Cl$ causes a drop in the total acidity of the support (Table 4) including strong acidity as the quantity of NH_3 desorbing above 350 °C is decreased as well (Fig. 11). This could explain the decrease in hydrocracking selectivities of trimetallic catalysts. On the other hand, although the constantly increased isomerization selectivities with increasing In loadings suggest an increase in the population of mild acidity sites

relative to that of strong sites, it was very difficult to distinguish the different sites observed by NH_3-TPD profiles.

Concerning dehydrocyclization, selectivities of both Pt/Al_2O_3Sn–Cl and Pt/Al_2O_3In–Cl to toluene are very close. A similar result has been found by Passos et al. [28]. Indium addition to Pt/Al_2O_3Sn–Cl does not seem to strongly affect toluene selectivity except at the highest In content (0.59 wt.%) where it is significantly lower (Table 5). Dehydrocyclization is accepted as a bifunctional mechanism in which the metal produces unsaturated intermediates that later undergo isomerization and ring closure steps on acidic sites of the support, on which the rate limiting steps are catalysed [49]. Therefore, the absence of indium effect on toluene selectivity for the first three catalysts could be explained by both the blockage of some Pt sites and the increase in isomerization selectivity, competing to tune the dehydrocyclization selectivity. Consequently, the decrease in toluene selectivity for Pt/Al_2O_3SnIn(0.59)–Cl is possibly due to the loss of catalytic activity by the more pronounced blockage of metal sites by indium.

4. Conclusions

In this work, we have prepared and characterized various trimetallic Pt/Al_2O_3SnIn–Cl naphtha-reforming catalysts with variable In loading in order to elucidate the effect of indium on the properties of the metallic function. Indium addition to the Al_2O_3Sn–Cl support weakens Sn-alumina interactions, possibly by the occupation of highly reactive alumina sites. This competition between indium and tin on active alumina sites leads to easier reduction of both metallic oxides under hydrogen as seen in temperature-programmed reduction. Furthermore, a strong Pt–In interaction is observed by TPR for all trimetallic catalysts, possibly occurring via formation of Pt_xIn alloys.

A fraction of tin is reduced to the metal state in the bimetallic Pt/Al_2O_3Sn–Cl catalyst, but alloying with platinum is not reached in the absence of indium, indicating that tin, even though reduced to the metal state, is still in a relatively strong interaction with alumina as suggest the hyperfine parameters of the reduced phase. Direct evidence on the formation of Pt_xSn alloys upon indium addition was obtained by ^{119}Sn Mössbauer spectroscopy characterization of trimetallic catalysts, in agreement with TPR results. The increase in the indium content was shown to be accompanied by an increase of Pt–Sn alloying. Results also revealed that Pt–Sn alloys formed at higher indium contents contained higher tin atomic concentrations.

FTIR–CO spectroscopy results show that the addition of indium or tin alone does not induce electronic modification of platinum centres, as seen in the case of the bimetallic Pt/Al_2O_3In–Cl and Pt/Al_2O_3Sn–Cl catalysts. This suggests that In is present either as a metallic unalloyed form or that Pt_xIn alloys (if formed) do not alter Pt electronic properties. This also indicates that unalloyed Sn^0 atoms do not exert an electronic effect on platinum. The slight decrease in the CO chemisorption capacities of these catalysts relative to the monometallic Pt catalyst is rather due to a geometric blockage of platinum sites by inert tin and indium atoms. Comparison of FTIR–CO and Mössbauer spectroscopy results obtained for bimetallic Pt/Al_2O_3Sn–Cl and trimetallic catalysts suggests that an electronic effect on platinum (when observed) is induced by tin only in the case of Pt–Sn alloying and that such an effect is more important when the tin content in the alloy is higher (case of catalysts with 0.39 and 0.59 wt.% In). Geometric effect on Pt atoms is in all cases acceptable by Sn in Pt–Sn alloys or Sn ions, and by In atoms in Pt_xIn alloys or In ions. This is consistent with STEM results, showing that at the highest In loadings the particles were slightly bigger. Thus, trimetallic catalysts at higher indium contents show progressively decreased chemisorption capacities, due to both geometric and electronic effect.

The results obtained from *n*-heptane reforming are consistent with the previous conclusions that the added indium interacts with both catalyst's metallic and acidic functions. The decrease in the total activity with increasing In contents is attributed to the physical blockage of Pt atoms due to indium presence and loss of acid sites on the support. The decrease in the hydrogenolysis (structure sensitive) selectivity is attributed to the formation of bimetallic alloys (Pt_xSn and possibly Pt_xIn) over which hydrogenolysis sites are passivated. The decrease in the hydrocracking selectivity and the increase of isomerization selectivity are consistent with an effect of In on the acidity of the support.

Acknowledgments

Ali Jahel would like to thank IFP and ANRT for research grants. Financial support by the Region Languedoc-Roussillon for the X-ray and γ-ray platform is also acknowledged.

References

[1] P.G. Menon, Z. Paal, Ind. Eng. Chem. Res. 36 (1997) 3282.
[2] V. Hansel, US Patents 2 479 101; 2 479 110, 1949 (to UOP).
[3] H.E. Kluksdahl, US Patent 3 415 737, 1968 (to UOP).
[4] French Patent 2 031 984, 1969 (to Compagnie Francaise de Raffinage).
[5] K.R. McCallister, T.P. O'Neal, French Patent 2 078 056, 1971 (to UOP).
[6] J.H. Sinfelt, US Patent 3 953 368, 1976 (to Exxon).
[7] F.M. Dautzenberg, J.N. Helle, P. Biloen, W.M.H. Sachtler, J. Catal. 63 (1980) 119.
[8] P. Biloen, J.N. Helle, H. Verbeek, F.M. Dautzenberg, W.M.H. Sachtler, J. Catal. 63 (1980) 112.
[9] R. Burch, J. Catal. 71 (1981) 348.
[10] R. Bacaud, P. Bussière, F. Figueras, J. Catal. 69 (1981) 399.
[11] V.I. Kuznetsov, A.S. Belyi, E.N. Yurchenko, M.D. Smolikov, M.T. Protasova, E.V. Zatolokina, V.K. Duplyakin, J. Catal. 99 (1986) 159.
[12] M.C. Hobson Jr., S.L. Goresh, G.P. Khare, J. Catal. 142 (1993) 641.
[13] L.D. Sharma, M. Kumar, A.K. Saxena, D.S. Rawat, T.S.R. Prasada Rao, Appl. Catal. A 168 (1998) 251.
[14] R. Burch, L.C. Garla, J. Catal. 71 (1981) 360.
[15] J.C. Serrano-Ruiz, A. Sepulveda-Escribano, F. Rodriguez-Reinoso, J. Catal. 246 (2007) 158.
[16] V.A. Mazzieri, J.M. Grau, C.R. Vera, J.C. Yori, J.M. Parera, C.L. Pieck, Catal. Today 107–108 (2005) 643.
[17] R.D. Cortright, J.M. Hill, J.A. Dumesic, Catal. Today 55 (2000) 213.
[18] V.A. Mazzieri, J.M. Grau, C.R. Vera, J.C. Yori, J.M. Parera, C.L. Pieck, Appl. Catal. A: General 296 (2005) 216.
[19] S.M. Stagg, C.A. Querini, W.E. Alvarez, D.E. Resasco, J. Catal. 168 (1997) 75.
[20] C. Carnevillier, F. Epron, P. Marecot, Appl. Catal. A: General 275 (2004) 25.
[21] L.S. Carvalho, C.L. Pieck, M.C. Rangel, N.S. Fígoli, J.M. Grau, P. Reyes, J.M. Parera, Appl. Catal. A: General 269 (2004) 91.
[22] L.S. Carvalho, C.L. Pieck, M.C. Rangel, N.S. Fígoli, C.R. Vera, J.M. Parera, Appl. Catal. A: General 269 (2004) 105.
[23] P.Y. Le Goff, F. Le Peltier, J. Giraud, S. Lacombe, C. Chau, French Patent 2 910 347, 2008 (to Institut Français du Pétrole).
[24] P.L. Bodgan, T. Imai, US Patent 5 858 908, 1999.
[25] S.A. Bocanegra, A.A. Castro, O.A. Scelza, S.R. de Miguel, Appl. Catal. A: General 333 (2007) 49.
[26] F.B. Passos, M. Schmal, M.A. Vannice, J. Catal. 160 (1996) 106.
[27] F.B. Passos, M. Schmal, M.A. Vannice, J. Catal. 160 (1996) 118.
[28] F.B. Passos, D.A.G. Aranda, M. Schmal, J. Catal. 178 (1998) 478.
[29] F.B. Passos, I.S. Lopes, P.R.J. Silva, H. Saitovitch, Catal. Today 78 (2003) 411.
[30] S.A. Bocanegra, P.D. Zgolicz, O.A. Scelza, S.R. de Miguel, Catal. Comm. 10 (2009) 1463.
[31] J. Olivier-Fourcade, M. Womes, J.C. Jumas, F. Le Peltier, S. Morin, B. Didillon, ChemPhysChem 5 (2004) 1734.
[32] W. Kundig, Nucl. Instrum. Methods 75 (1969) 336.
[33] M. Primet, J. Catal. 88 (1984) 273.
[34] P.W. Park, C.S. Ragle, C.L. Boyer, M.L. Balmer, M. Engelhard, D. McCready, J. Catal. 210 (2002) 97.
[35] J.A. Perdigon-Melon, A. Gervasini, A. Auroux, J. Catal. 234 (2005) 421.
[36] V.A. Mazzieri, C.L. Pieck, C.R. Vera, J.C. Yori, J.M. Grau, Appl. Catal. A: General 353 (2009) 93.
[37] H. Lieske, G. Lietz, H. Spindler, J. Volter, J. Catal. 81 (1983) 8.
[38] S.R. de Miguel, O.A. Scelza, A.A. Castro, Appl. Catal. 44 (1988) 23.
[39] M. Womes, F. Le Peltier, S. Morin, B. Didillon, J. Olivier-Fourcade, J.C. Jumas, J. Mol. Catal. A: Chem. 266 (2007) 55.
[40] R. Srinivasan, B.H. Davis, Plat. Metall. Rev. 36 (1992) 151.
[41] G.J. Siri, J.M. Ramallo-Lopez, M.L. Casella, J.L.G. Fierro, F.G. Requejo, O.A. Ferretti, Appl. Catal. A: General 278 (2005) 239.
[42] F. Humblot, B. Didillon, F. Lepeltier, J.P. Candy, J. Corker, O. Clause, F. Bayard, J.M. Basset, J. Am. Chem. Soc. 120 (1998) 137.

[43] C. Vertes, E. Talas, I. CzakoNagy, J. Ryczkowski, S. Gobolos, A. Vertes, J. Margitfalvi, Appl. Catal. 68 (1991) 149.
[44] J.C. Serrano-Ruiz, G.W. Huber, M.A. Sánchez-Castillo, J.A. Dumesic, F. Rodríguez-Reinoso, A. Sepúlveda-Escribano, J. Catal. 241 (2006) 378.
[45] R. Barth, R. Pitchai, R.L. Anderson, X.E. Verykios, J. Catal. 116 (1989) 61.
[46] R. Barth, A. Ramachandran, J. Catal. 125 (1990) 467.
[47] H. Verbeek, W.M.H. Sachtler, J. Catal. 42 (1976) 257.
[48] C. Dupont, D. Loffreda, F. Delbecq, F.J. Cadete Santos Aires, E. Ehret, Y. Jugnet, J. Phys. Chem. C 112 (2008) 10862.
[49] V.M. Benitez, C.R. Vera, M.C. Rangel, J.C. Yori, J.M. Grau, C.L. Pieck, Ind. Eng. Chem. Res. 48 (2009) 671.
[50] V. Rodríguez-González, R. Gómez, M. Moscosa-Santillan, J. Amouroux, J. Sol–Gel. Sci. Technol. 42 (2007) 165.
[51] V. Ponec, Adv. Catal. 32 (1983) 149.
[52] P. Mériaudeau, A. Thangaraj, J.F. Dutel, P. Gelin, C. Naccache, J. Catal. 163 (1996) 338.
[53] P. Mériaudeau, C. Naccache, A. Thangaraj, C.L. Bianchi, R. Carli, S. Narayanan, J. Catal. 152 (1995) 313.